G_0-G_1 cell cycle phase transition as revealed by fluorescence resonance energy transfer: analysis of human fibroblast chromatin

G. Bottiroli, A.C. Croce, M.G. Bottone, S. Vaccino, C. Pellicciari
Istituto di Genetica Molecolare del CNR, Sezione di Istochimica e Citometria, and Dipartimento di Biologia Animale, University of Pavia, Italy

In the present study, microspectrofluorometry and digital imaging procedures were used to investigate by fluorescence Resonance Energy Transfer (FRET) analysis the changes of chromatin organization during the transition from G_0 quiescent state to G_1 phase. G_0-G_1 transition is a key event in cell cycle progress depending on the activation of specific genes and the concomitant silencing of others, which both entail spatial chromatin rearrangement. Normal human fibroblasts arrested in G_0-phase by culture in low-serum contanining medium and stimulated to re-enter G_1 by serum addition were used as cell model. To investigate the occurrence and timing of these supramolecular chromatin changes, we estimated the relative FRET efficiency in single cells after double-staining with two DNA-specific dyes which non-covalently bind to double-helical DNA. Hoechst 33258 and propidium iodide were used as a donor-acceptor dye pair since they exhibit particularly favourable spectral characteristics, that allow the calculation procedure to be semplified. The results of FRET analysis were compared to those of the immunocytochemical labelling of two nuclear proteins (i.e., Ki-67 and statin) whose expression is an established marker of potentially proliferating G_1 cells or resting G_0 cells, respectively. FRET efficiency was lower in G_0 than in G_1 fibroblasts: this is likely due to a higher chromatin packaging in quiescent cells which especially hinders the intercalation of propidium iodide molecules, thus making the interaction with the donor molecules less favourable, in terms of relative distance and spatial orientation. FRET efficiency significantly increased shortly (1h) after serum stimulation of quiescent fibroblasts, thus indicating that chromatin is rearranged in parallel with activation of cycle-related gene; it is worth noting that these signs largely preceded the occurrence of immunopositivity for Ki-67, which was detectable only 24h after serum stimulation. FRET-based analyses, which already proved to be suitable for studying the overall chromatin organization in differentiated cells, may now be envisaged as a powerful tool for detecting, in single cells, more subtle changes linked to the activation of early cycle-related genes.

Key words: chromatin, fluorescence resonance energy transfer (FRET), G_0-G_1 transition, Hoechst 33258 human fibroblasts, propidium iodide.

Correspondence: Giovanni Bottiroli, Istituto di Genetica Molecolare del CNR, Sezione di Istochimica e Citometria, piazza Botta 10, 27100 Pavia, Italy.
E-mail: botti@igm.cnr.it

Paper accepted January 12, 2004

European Journal of Histochemistry
2004; vol. 48:37-48

Non radiative fluorescence resonance energy transfer (FRET) is a photophysical phenomenon which can occur between two fluorochromes exhibiting favourable spectral characteristics. According to Forster's theory (Forster, 1948), the excitation energy of one fluorochrome (acting as the donor) can be transferred to a second one (the acceptor), the efficiency of the process being dependent on factors such as fluorochrome distance, reciprocal orientation, and spectral overlapping. Information on the supramolecular spatial arrangements of biological substrates can be obtained from FRET efficiency analysis, provided that the donor and the acceptor dyes bind the biomolecules under study with high specificity (Stryer, 1978).

Specific labelling toward target structures was obtained with donor- and acceptor-tagged antibodies or lectines, to investigate plasma membrane structure (Matkò et al., 1988; Szöllõsi et al., 1984, 1987; Locatelli et al., 1998; Nagy et al., 1998), or protein interaction during apoptosis (Gordon et al., 1998). More recently, the availability of a class of genetically encoded autofluorescent proteins provided a powerful tool for studying protein interaction in living cells by FRET (Heim and Tien, 1996; Kim et al., 2003).

Direct labelling with DNA specific dyes was applied to investigate the structural arrangements of chromatin in metaphase chromosomes (Sahar and Latt, 1980; Latt et al., 1980; Langlois and Jensen, 1979) or in interphase nuclei (Bottiroli et al., 1989, 1994).

In steady-state microscopy, the approaches generally applied to evaluate FRET efficiency are based on the measurement of either the donor photobleaching (Jovin and Arnt-Jovin, 1989), the donor fluorescence decay time (Murata et al., 2000a), the donor fluorescence quenching (Uster and Pagano, 1986), or the sensitized emission of the acceptor. This lattest approach can be performed using microspectrofluorometry, fluorescence imaging and

flow cytometry (Clegg, 1996; Szöllõsi et al., 1998). It requires spillage factors to be introduced to exclude or minimize the interferences arising from sample autofluorescence, acceptor excitation at the donor excitation wavelength, and donor emission at the acceptor emission range (Kam et al. 1995, Nagy et al., 1998, Gordon et al., 1998).

For donor-acceptor dye pairs with particularly favourable spectral properties, the analytical procedure can be significantly semplified. This approach was successfully applied to study the superstructural modifications of the DNA-protamine complex in spermatozoa during spermiogenesis (Bottiroli et al., 1994) or after exposure to chemical or physical agents (Zuccotti et al., 1994).

Cell cycle related chromatin changes were recently shown in G_1 and G_2-M phase cells, through a FRET investigation of the spatial distribution of AT- and GC-rich regions, after labelling with the specific fluorochromes, Hoechst 33258 and 7-amino-actinomycin-D respectively (Murata et al., 2003).

In the present study, microspectrofluorometry and digital imaging procedures have been used to investigate by FRET analysis the cell-cycle-related changes of chromatin organization during the transition from the G_0 quiescent state to G_1 phase. This is a key event in the cell cycle progress, the entrance of a cell into the pre-DNA synthetic phase depending on the activation of specific genes and the concomitant silencing of others, which both entail spatial chromatin rearrangement (reviewed in Leitch, 2000). Normal human fibroblasts kept in G_0-phase by growth in low-serum containing medium and stimulated to re-enter G_0 by serum addition were used as a cell model.

To investigate the occurrence and timing of these supramolecular chromatin changes, we estimated the relative FRET efficiency in single cells after double-staining with two DNA-specific dyes which non-covalently bind to double-helical DNA, Hoechst 33258 (Ho258) and propidium iodide (PI). This donor-acceptor dye pair was already used to study chromatin composition and organisation in chromosomes (Sahar and Latt, 1980; Latt et al., 1980; Langlois and Jensen, 1979; Ronchetti et al., 1997). These dyes have small competitive or cooperative binding, as Ho258 is an AT-base specific non-intercalating agent that binds the minor grove of the DNA double helix, whereas PI is a base unspecific dye that intercalates between DNA bases (Le Pecq and Paoletti, 1967). Assuming that Ho258 and PI do not bind to the same base pairs, the minimal distance between the centers of the donor and acceptor dye molecules was estimated to be about 13 Å (Murata et al., 2000b); modification of chromatin superstructure may be expected to induce changes in the donor-acceptor distance, thus affecting the efficiency of the energy transfer process.

The results of FRET analysis have been considered in comparison with those of the immunocytochemical labelling of two nuclear proteins (i.e., Ki-67 and statin) whose expression is an established marker of potentially proliferating G_1 cells or resting G_0 cells, respectively. Ki-67 antigen was shown to be absent in G_0 cells, while being expressed at increasing levels during G_1, S and G_2/M phase (Santisteban and Brugal, 1995, Endl et al., 1997; Mangiarotti et al., 1998). On the contrary, statin is expressed in kinetically quiescent cells, as originally observed in senescent fibroblasts (Wang, 1985a) and in young fibroblasts after serum starvation or contact inhibition (Wang 1985b; Pellicciari et al., 1995); this proved to occur also in normal and tumor tissues *in vivo* (Wang and Krueger, 1995; Pellicciari et al., 1995). Statin immunopositivity decreases after the cells have re-entered the proliferation cycle, although in fibroblasts statin completely disappears from the nucleus only after 72 h (Wang and Lin, 1986).

Materials and Methods

Chemicals

Ho258 and PI (Sigma Chem. Co., St. Louis, MO, USA) were prepared as stock solutions in distilled water at the concentrations of 1 mg/mL and 500 µg/mL, respectively. Prior to use, the final dilutions were performed in phosphate buffer (pH 6.85, 0.1 M) containing either 0.4 M NaCl or 20 mM $MgCl_2$ for Ho258 and PI, respectively.

Cell cultures

Normal human fibroblasts – passages 4 to 15 – were grown in DMEM (Dulbecco Modified Eagles Medium), supplemented with fetal bovine serum (FBS), 2 mM glutamine and 100 units/ml of streptomycin and penicillin. Cell conditions: i) asynchronously cycling fibroblasts grown at low cell density in DMEM supplemented with 10% FBS, seeded three days before measurements; ii) resting (G_0) cells from cultures kept for al least 7 days in DMEM supplemented by 0.5% FBS (Pellicciari et

al., 1995); iii) G_1 fibroblasts obtained by trasferring G_0 fibroblasts to a medium contaning 10% FBS for different times (30 min to 24h).

For flow cytometry, cells grown in 25 cm^2 flasks were detached by mild trypsinization (0.5% trypsin in PBS containing 0.2% EDTA), washed in PBS and fixed for 15 min with 70% ethanol at 4C°. For microspectrofluorometry, cells were grown on glass coverslips in multiwell plates, washed in PBS and fixed, as above; before staining, the cells were rehydrated with PBS and treated with RNase type A (100 U/ml in PBS, 2 h at room temperature; Sigma, Chem. Co.).

All the culture media, sera and disposable plastics were from Celbio s.r.l. (Milano, Italy).

Cell cycle analysis

Cycle phase cell distribution was defined *via* DNA cytofluorometry on trypsinized unfixed cells, stained in suspension for 30 min with 50 µg/mL of PI in distilled water containing RNase type A (100 U/mL) and 0.001% Nonidet NP40.

The percentage of S-phase fibroblasts in the different culture conditions was estimated by bromodeoxyuridine incorporation experiments, according to the procedure previoulsy described (Lanni et al., 2003).

Cycle-related proteins were detected immunocytochemically on ethanol-fixed cells; after rehydration in PBS containing 0.1% bovine serum albumin and 0.5% Tween 20, the cells were incubated for 1 hr at room temperature with mouse monoclonal antibodies recognizing either the nuclear antigen Ki-67 (Myb1: Dako S.p.A., Milan, Italy) or statin (kind gift of dr. Eugenia Wang), and then with an FITC-conjugated anti-mouse IgG goat-antibody. The immunolabeled cell samples were finally counterstained for DNA with 5 µg/mL of PI for 15 min. Flow cytometric measurements were performed with a FACStar (Becton Dickinson, San José, CA, U.S.A.) equipped with argon laser excitation at 488 nm (power 200 mW), 510-540 nm interference filter for the green fluorescence signals of FITC-conjugated antibodies and 610 nm long-pass filter for the red fluorescence signals. The percentage of FITC-positive cells was estimated by rectangular-region analysis on dual-parameter scattergrams. As a background fluorescence control, the primary antibody was omitted in some samples. At least 20,000 cells were contained in the gated regions used for calculations.

Ho258/PI-DNA binding sites

The amount of dye molecules bound to DNA (dye-DNA) was estimated experimentally through binding kinetic studies, assuming the binding sites to be equal and independent for each dye, according to the equation:

$$[\text{dye-DNA}] = N\,[\text{dye}]/(Kd + [\text{dye}])$$

where N is the total binding sites occupied, [dye] the free ligand concentration and Kd the dissociation constant.

Exploiting the fact that both Ho258 and PI dyes become fluorescent upon binding to DNA, the number of binding sites can be derived from the Benesi-Hildebrand equation, plotting the reciprocal of the initial reaction velocity ($v = d[\text{dye-DNA}]/dt$) — expressed as fluorescence intensity counts/sec — *versus* the reciprocals of the free dye concentrations, according to the Lineweaver-Burk plot, usually applied to enzyme kinetics (Marshall, 1978). The plot of 1/v against 1/[dye] gives a straight line with an intercept of the x axis of (–1/Kd) and an intercept of the y axis of (1/N). The free ligand concentration can be approximated to the concentration of the total ligand (Price and Dwek, 1979), since in our experimental conditions the concentrations of Ho258 and PI are in considerable excess over DNA concentration.

To make the reaction velocity comparable in terms of dye concentration, the fluorescence intensity counts were calculated as the whole integrals of the spectra corrected for both the excitation wavelength intensity and the detector sensitivity, normalized for both the absorption coefficient of the two dyes at their wavelengths (405 and 546 nm), and for the dye quantum efficiencies (Table 1), and expressed as concentration units (c.u.).

Experimentally, Ho258 and PI were diluted in buffer solutions to concentrations from 0.2 to 2 µg/ml, and from 1 to 10 µg/mL, respectively. Unstained single cells adherent to the upper side of the slides, previously fixed and treated with RNase as described above, were immersed in phosphate buffer, centred and focused under bright field by a water immersion objective (Carl Zeiss, 40 X, N.A. 0.75). The buffer was removed and replaced with Ho258 or PI staining solutions and fluorescence intensity-*versus*-time curves were recorded by means of the microspectrofluorometer described below.

Table 1. Ho258 and of PI spectroscopic parameters.

	λ	I_0 rel	ε	ϕ
PI Acceptor	405	1	754°	0.13*
	546	3.1°	5420°	
Ho258 Donor	405	1	3700°	0.42*

*°Measured in the present work; *from Cosa et al., 2001.*

Plotting of the experimental data gives the following values: $Ho258_{G0}$: N = 0.573 c.u., Kd = 2.93×10^{-6} M; $Ho258_{G1}$: N = 0.451 c.u., Kd = 1.55×10^{-6} M; PI_{G0}: N = 0.190 c.u., Kd = 1.49×10^{-5} M : PI_{G1}: N = 0.163 c.u., Kd = 0.95×10^{-5} M.

Considering that the dye concentrations used in the FRET efficiency analysis were 3.2×10^{-6} M and 1.5×10^{-5} M for Ho258 and PI respectively, the following [dye-DNA] values were obtained: $Ho258_{G0}$ = 0.299, $Ho258_{G1}$ = 0.304, PI_{G0} = 0.095, PI_{G1} = 0.102.

Ho258 and PI single- and double-cell staining

FRET analysis was performed on cells adhering to coverslips fixed in ethanol, treated with RNase as reported above, and stained with Ho258 and PI at the final concentrations of 2 µg/ml (3.2×10^{-6}M), and 10 µg/ml (1.5×10^{-5}M), respectively. PI staining (10 min) was followed by rinsing in the dye-free phosphate buffer, staining with Ho258 dye solution (20 min), and rinsing in the dye-free buffer (10 min). The slides were mounted in the buffer solution and sealed, to prevent drying of the samples. For single-stained samples, the same procedure was followed except that, for either dye, the solution of the other fluorophore was substituted by the pure buffer.

Spectrofluorometric analysis

For spectral analysis in solution, Ho258 and PI were diluted in the respective buffers to 10 µg/ml (1.6×10^{-5}M) and 25 µg/ml (3.75×10^{-5}M) concentration, in the presence of a fifty times higher concentration of calf thymus DNA. Fluorescence spectra were recorded with a spectrofluorometer (model SP2, Applied Photophysics, Leatherhead, UK), equipped with a photomultiplier tube (model 9558/Q, Thorn –EMI Electronic Tube Ltd., Ruislip, England), and with a photon counting system (EG&G-Ortec, Berks, England). A 150 W xenon lamp (Osram, Berlin, Germany) was used as an excitation source. The excitation and emission spectra were recorded in the 300-730 nm range.

Table 2. Optical filters and measurements conditions.

	Excitation interferential filters (Hg 100W lamp lines)	*Dichroic mirror*	*Emission Spectral Analysis Long pass filter*	*Image Analysis*
Autofluorescence ($AF_{366/480}$)	366 nm (FWHM 7 nm)	TK405 ($T\%_{405}$ = 10)	430 nm	480 ± 10% interferential filter
Donor Ho258 ($I_{405/480}$)	405 nm (FWHM 4 nm)	TK405 ($T\%_{405}$ = 10)	430 nm	480 ± 10% interferential filter
$FRET_{405/630}$	405 nm (FWHM 4 nm)	TK405 ($T\%_{405}$ = 10)	430 nm	610 Long pass filter
Acceptor PI ($I_{546/630}$)	546 nm (FWHM 5 nm)	TK550 ($T\%_{550}$ = 10)	610 nm	610 Long pass filter

FRET analysis, microspectrofluorometry

Microspectrofluorometric analysis was performed under epi-illumination by means of a microspectrograph (Leitz, Wetzlar, Germany), equipped with an optical multichannel analyzer using a 512 element intensified linear diode array detector (OMA III - EG&G-PRA, Princeton, NJ, USA). The excitation light was provided by a 100W high-pressure Hg lamp, combined with KG1 and BG38 antithermal filters. Fluorescence measurement conditions are summarized in Table 2. All the measurements were performed using a Leitz 40X NPL Neofluotar (NA 1.30) oil-immersion objective. On-line subtraction of background contribution due to dark current and the optical equipment emission was performed during recording of data.

FRET analysis, imaging

Single cell fluorescence images were recorded under epi-illumination conditions using a Hamamatsu C2400-09 ISIT camera (Hamamatsu Photonics Deutschland GmbH, Herrsching am Ammersee, Germany), mounted on a Leitz Orthoplan fluorescence microscope. A Leitz Neofluar 100 X oil-immersion iris objective (NA 1.32-0.60) was employed. Images were acquired under the conditions reported in Table 2.

Calculations between images were performed pixel-by-pixel by means of the software provided by the Argus 100 control program (Hamamatsu Photonics Deutschland GmbH, Herrsching am Ammersee, Germany).

Image generated by the camera dark current and by the fluorescence of both microscope optical elements and coverslip were registered in cell free areas of each sample and subtracted pixel-by-pixel from each sample image. Images were corrected for

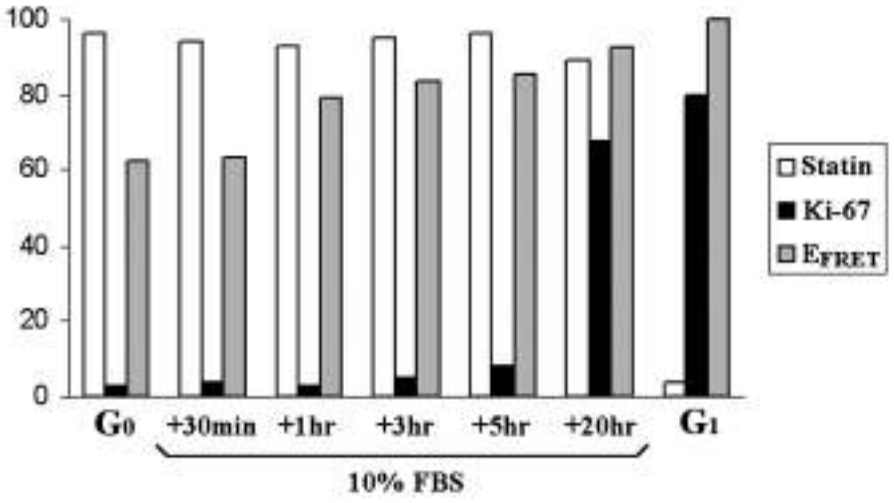

Figure 1. Human fibroblasts under quiescent (G_0), and cycling (G_1) condition, and during the release from the quiescent state: percentage of statin- or Ki-67-positive fibroblasts, and relative FRET efficiency (E_{FRET}) obtained according to equation (14), where C(A)/C(D) values were calculated as fluorescence intensity ratio; FRET values were normalized to the G_1 FRET value.

the shift of position, due to the use of different dichroic mirrors. Background-subtracted images were submitted to pixel-by-pixel FRET calculation according to Equation (14) (see Results).

The images were processed for colour presentation and printing by means of Scion Image for Windows (Scion Co., Frederik, Ma., USA).

For each image the averaged values were computed, and the single pixel FRET values were grouped and presented as distribution histograms. For each cell, the symmetry of the data distribution profile, which followed a two half Gaussians distribution, was analyzed by means of the GMG (half-Gaussian Modified Gaussian) asymmetry parameter provided by the PeakFit™ programm (SPSS Inc., Surrey, UK). With reference to the maximum frequency value, this parameter is equal to 1 when the two areas at the left and right of the maximum are equal (ideal symmetry), increases to values > 1 at the increasing of the half area at the right side, and decreases to values < 1 at the increasing of the area at left.

Results

Cytokinetic characteristics

Fibroblasts under the different growth conditions used were examined by fluorescence microscopy and cytometry, following immunodetection of Brdu incorporation, and of Ki-67 and statin. In fibroblast cultures grown in medium containing 10% FBS, about 12% of the cells were in the S-phase and more than 90% of the cells were Ki-67 positive, whereas less than 5% were statin positive, resting cells (Figure 1). After at least 7 days culture in low-serum-containing medium, S-phase cells were less than 0.5%, almost all the cells had 2C DNA content; less than 5% of the cells were labelled for Ki-67, whereas more than 95% were positive for statin. These two culture conditions, therefore, proved to be suitable to obtain almost pure populations of either cycling or resting fibroblasts, in which G_1 and G_0 cells respectively were easily identified as the cells with 2C DNA content.

Following serum stimulation of resting cultures (Figure 1), the percentage of Ki-67-positive fibroblasts increased with increasing stimulation time; after 24h Ki-67-positive cells were similar as in the cycling fibroblast cultures. The percentage of statin-positive cells decreased progressively but slightly after 24h: this is consistent with previous observations on a similar model system, as already recalled (Wang, 1985a).

Spectrofluorimetric analysis

Typical examples of Ho258 and PI fluorescence excitation and emission spectra, recorded in solution in the presence of an excess concentration of DNA, are shown in Figure 2. Excitation and emission bands of Ho258 cover the 300-430 nm and the 380-600 nm ranges, respectively. The excitation spectrum of PI is characterized by a band in the 450-580 nm region, in addition to an increasing tail at wavelengths shorter than 400 nm, the minimum values being found in the 400-410 nm range. The PI emission band covers the 550-730 nm region. A

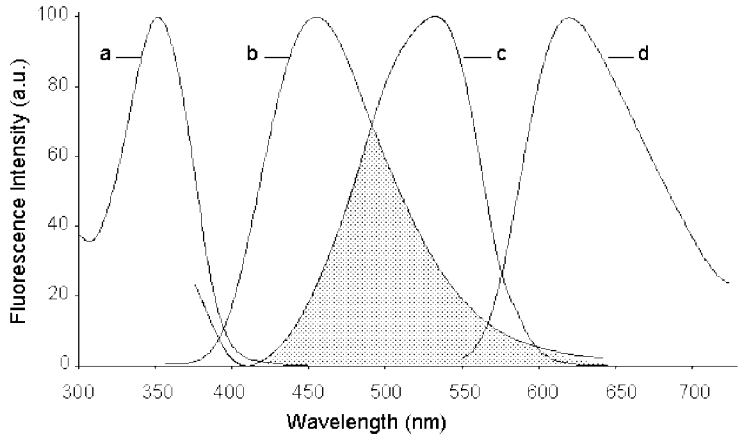

Figure 2. Typical examples of excitation and emission spectra of Ho258 (a and b, respectively), and PI (c and d, respectively), in solution in the presence of an excess of calf thymus DNA. Shaded area: overlapping region.

superimposition area between the emission spectrum of Ho258 and the excitation of PI is found in the 450-550 nm region.

Figure 3A reports typical examples of the fluorescence emission spectra recorded by microspectrofluorometry from single- and double- stained cells. Under excitation at 405 nm, cells submitted to single staining with Ho258 show the main emission band in the 430-600 nm region. The same excitation condition on single PI stained cells gives rise to two broad emission bands, in the 430-550 nm and 580-680 nm regions, that can be ascribed to the cell autofluorescence and to PI direct emission, respectively. The intensity value of this latter at 630 nm corresponded to 7% of the PI emission of the same cell under 546 nm excitation. In the double stained cells excitation at 405 nm results in an emission characterized by two bands in the 430-580 nm and 580-680 nm regions, that can be attributed to the direct emission of the donor and of the sensitized plus the direct emission of the acceptor, respectively (Figure 3B).

FRET efficiency calculation

FRET efficiency can be calculated from the acceptor sensitized emission according to the equation (Dale and Eisinger, 1975, Schiller 1975):

$$E = \left(\frac{{}_{405}FI\,(A_{D/A})_{630}}{{}_{405}FI\,(A_A)_{630}} - 1\right) \cdot \frac{\varepsilon\,(A)_{405}\,C\,(A)}{\varepsilon\,(D)_{405}\,C\,(D)} \qquad \textbf{(1)}$$

where ${}_{405}FI\,(A_{D/A})_{630}$ and ${}_{405}F(A_A)_{630}$ are the fluorescence intensities of the acceptor PI, measured at 630 nm under excitation at 405 nm, in the presence ($A_{D/A}$) or in the absence (A_A) of the donor Ho258, and $\varepsilon_{405}C(A)$ and $\varepsilon_{405}C(D)$ correspond to the absorbance values of the acceptor and of the donor at the donor wavelength.

Table 3 lists each of the symbols used in the analysis of the FRET data.

Due to partial overlap between the excitation and emission spectra of the donor and acceptor fluo-

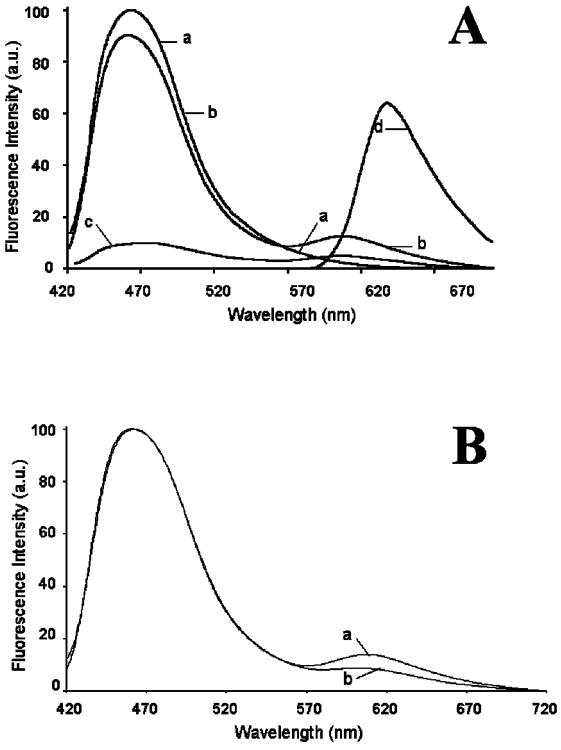

Figure 3. A: Typical examples of emission spectra of Ho258, and PI under different excitation conditions measured on single and double stained G_1 fibroblasts. Ho258 single staining, exc. 405 nm (a); Ho258/PI double staining, exc. 405 nm (b); PI single staining, exc. 405 nm (c); Ho258/PI double staining, exc. 546 nm (d). Emission amplitudes are normalized to (a) maximum value. B: Typical examples of emission spectra of Ho258, and PI under 405 nm excitation, measured on double stained G_1(a) and G_0 (b) fibroblasts.

Table 3. Symbols used in equations for FRET calculation and their description.

Symbol	*Dye present*	*Signal meaning*
$_{\lambda exc}AF_{\lambda exm}$	None	Autofluorescence
$I_{(D, A, D/A)\ \lambda exc/\lambda exm}$	Single ($_{(D,A)}$) or double ($_{(D,A)}$) stained samples	Fluorescence intensity experimentally measured under λexc/λexm conditions
$_{\lambda exc}\ FI(AF)_{\lambda exm}$	None	Contribution of named fluorochrome under λexc/λexm conditions
$_{\lambda exc}\ FI(D_D)_{\lambda exm}$	Donor	
$_{\lambda exc}\ FI(A_A)_{\lambda exm}$	Acceptor	
$_{\lambda exc}\ FI\ (D_{D/A})/_{\lambda exm}$	Donor in the presence of the Acceptor	
$_{\lambda exc}\ FI\ (A_{D/A})/_{\lambda exm}$	Acceptor in the presence of the Donor	

Symbol	*Correction factors*	*Dye*
$z = {}_{\lambda exc1}FI(AF)_{\lambda exm}/{}_{\lambda exc2}FI(AF)_{\lambda exm}$	Correction factor for autofluorescence contribution at measuring λ	Autofluorescence
$k = {}_{\lambda exc1}FI(D_D)_{\lambda exm}/{}_{\lambda exc2}\ FI(D_D)_{\lambda exm}$	Autofluorescence correction factor for the Donor at each related λ	Donor
$k' = {}_{\lambda exc1}FI(A_A)_{\lambda exm}/{}_{\lambda exc2}\ FI(A_A)_{\lambda exm}$	Autofluorescence correction factor for the Acceptor at each related λ	Acceptor
a, b, c, d.	Spillage factors (see Table 4)	

rophores, the fluorescence intensities measured at 630 nm under excitation at 405 nm contain more than one spectral component contribution. To estimate each single contribution, measurements must be performed under different excitation/emission conditions on double- and single-stained samples.

The measurements taken on double stained-samples are:

1) the fluorescence intensity in the donor emission range under excitation at the donor wavelength ($I_{405/480}$);

2) the fluorescence intensity in the acceptor emission range under excitation at the donor wavelength ($I_{405/630}$);

3) the fluorescence intensity in the acceptor emission range under excitation at the acceptor wavelength ($I_{546/630}$).

$I_{405/480}$ results from the contributions of the donor emission quenched by energy transfer [$_{405}FI(D_{D/A})_{480}$], of the cell autofluorescence [$_{405}AF_{480}$] and, possibly, of acceptor emission [$_{405}FI(A_{D/A})_{480}$]:

(2)

$$I_{405/480} = {}_{405}FI(D_{D/A})_{480} + {}_{405}AF_{480} + {}_{405}FI(A_{D/A})_{480}$$

$I_{405/630}$ results from the contributions of acceptor sensitized emission [$_{405}FI_s(A_{D/A})_{630}$], of the acceptor direct emission [$_{405}FI_d(A_{D/A})_{630}$], of the donor emission quenched by energy transfer [$_{405}FI(D_{D/A})_{630}$] and of the cell autofluorescence [$_{405}AF_{630}$]:

(3)

$$I_{405/630} = {}_{405}FI_s(A_{D/A})_{630} + {}_{405}FI_d\,(A_{D/A})_{630} + {}_{405}FI(D_{D/A})_{630} + {}_{405}AF_{630}$$

$I_{546/630}$ results from the contributions of the acceptor direct emission [$_{546}FI_d(A_{D/A})_{630}$], of the cell autofluorescence [$_{546}AF_{630}$] and, possibly, of the donor emission quenched by energy transfer [$_{546}FI(D_{D/A})_{630}$]:

(4)

$$I_{546/630} = {}_{546}FI_d(A_{D/A})_{630} + {}_{546}AF_{630} + {}_{546}FI(D_{D/A})_{630}$$

The net dye contribution can be evaluated by means of spectroscopic factors (spillage coefficients) calculated on single-stained samples according to the following equations:

(5)

$$a = {}_{405}FI(A)_{480}/{}_{546}FI(A)_{630}$$

(6)

$$b = {}_{405}FI(D)_{630}/{}_{405}FI(D)_{480}$$

(7)

$$c = {}_{405}FI(A)_{630}/{}_{546}FI(A)_{630}$$

Their values are summarized in Table 4.

The cell autofluorescence contribution to the donor and acceptor emissions can be estimated through calculation which must take into account that in the case of Ho258/PI dye pair there is no spectral range where autofluorescence is selectively excited. In such a situation the cell autofluorescence contributions can be evaluated on single-stained samples measuring the fluorescence intensity at the

Table 4. Spectroscopic factors for intensity-based energy transfer calculation.

Autofluorescence		*Dyes*			
		Donor		*Acceptor*	
K	1.110	b	0.01	a	nd
		$IF(D)_{405/630}/IF(D)_{405/480}$		$IF(A)_{405/480}/IF(A)_{546/630}$	
Z	2.450				
		d	nd	c	0.07
W	0.104	$IF(D)_{546/630}/IF(D)_{405/630}$		$IF(A)_{405/630}/IF(A)_{546/630}$	

°For $IF(A)_{405/480}$ and $IF(D)_{546/630}$ the intensity of cells was not distinguishable from the background, and thus the related spillage factors are neglected.

following excitation/emission condition: 366/480 and 405/480 for Ho258 and 366/630 and 546/630 for PI.

The fluorescence intensities measured on Ho258 stained cells concern:

(8)

$$_{405}I(D_D)_{480} = {}_{405}FI\,(D_D)_{480} + {}_{405}FI\,(AF)_{480}$$

(9)

$$_{366}I(DD)_{480} = {}_{405}FI\,(D_D)_{480} \cdot k + {}_{405}FI\,(AF)_{480} \cdot z$$

were k is determined on Ho258-DNA complex as the ratio of the fluorescence intensities at 480 nm under excitation at 366 and 405 nm, respectively $[k=I_{366/480}/I_{405/480}]$, and z is determined on unstained cells as the ratio of the fluorescence intensities at 480 nm under excitation at 366 and 405 $[k=I_{366/480}/I_{405/480}]$.

Solving the equations (8) and (9) gives:

(10)

$$_{405}FI(AF)_{480} = [{}_{336}FI(D_D)_{480} - {}_{405}FI(D_D)_{480} \cdot k]/[z - k]$$

Since the autofluorescence spectrum profile of the cells is fairly constant, the autofluorescence contribution at 630 nm under the same excitation condition, $_{405}FI(AF)_{630}$, can be calculated multiplying the result of equation (10) by the factor $w = [{}_{405}I_{630}/{}_{405}I_{630}]$ obtained from unstained cells:

(11)

$$_{405}FI(AF)_{630} = {}_{405}FI(AF)_{480} \cdot w$$

The fluorescence intensities measured on PI stained cells concern:

(12)

$$_{546}I(A_A)_{630} = FI_{546}\,(A_D)_{630} + FI_{546}(AF)_{630}$$

(13)

$$_{366}I(A_A)_{630} = FI_{546}\,(A_A)_{630} \cdot k' + FI_{546}(AF)_{630} \cdot z'$$

were k′ is determined on PI-DNA complex as the ratio of the fluorescence intensities at 630 nm under excitation at 366 and 546 nm, respectively $[k = I_{366/630}/I_{546/630}]$, and z′ is determined on unstained cells as the ratio of the fluorescence intensities at 630 nm under excitation at 366 and 546 $[k = I_{366/630}/I_{546/630}]$. Actually the cell autofluorescence contribution under excitation at 546 nm was neglected, since it is not distinguishable from the background, in agreement with the fact that absorbtion of most of the endogenous fluorophores occurs almost esclusively in the UV-blue spectral region. Spectroscopic factors are reported in Table 4.

Solving the equation (1), we obtain the equation (14) reported below.

To evaluate the FRET efficiency according to the equation (14) we need to calculate the ratio of the amount of light absorbed by the acceptor and the donor, as expressed by the factor $[\varepsilon_{405} \cdot C(A)]/[\varepsilon_{405} \cdot C(D)]$. The amount of absorbed light depends on the spectral profile of the fluorophores, on the properties of the excitation source and on the characteristics of the optics in the excitation wavelength range, and on the concentration of the fluorophores.

When the excitation occurs by means of a continuous spectrum source, all the above factors play an important role to define the total amount of absorbed photons by each of the two dyes. In that case, the total amount of absorbed photons is defined by the area of the product of the spectral profiles of all the components, as described by Nagy et al. (1998).

In the case of a sharp-line excitation source — as it can be assumed in our case with the 405 nm Hg line (FWHM = 4 nm, about 93% of energy within 9 nm) — the total amount of photons absorbed by

(14)

$$E = \left\{ \frac{I_{405/630} - {}_{405}AF_{630} - [(I_{405/480}) - {}_{405}AF_{480} - (I_{546/630} - {}_{546}AF_{630}) \cdot a] \cdot b}{(I_{546/630} - {}_{546}AF_{630}) \cdot c} - 1 \right\} \frac{\varepsilon(A)_{405} \cdot C(A)}{\varepsilon(D)_{405} \cdot C(D)}$$

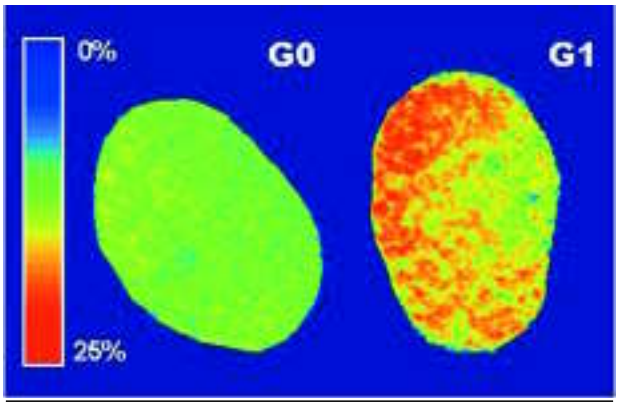

Figure 4- FRET image analysis. Typical topological patterns of FRET efficiency values in G_0 and G_1 fibroblasts obtained by means of pixel by pixel images calculation.

each dye can be considered proportional to the product of the absorption coefficient at 405 nm by the concentration. The absorption coefficient at 405 nm was calculated from Ho258- and PI- DNA complex solutions, giving the values of 7.54×10^2 and 3.70×10^3 dm^3 mol^{-1} cm^{-1} for PI and Ho258, respectively. The dye concentrations in the nuclei were estimated by binding kinetics studies, as described in Materials and Methods. For the dye concentrations used in the FRET efficiency analysis, the following acceptor/donor concentration ratios are obtained: $[C(A)/C(D)]G_0 = 0.318$, $[C(A)/C(D)]G_1 = 0.335$.

Table 5 summarizes the mean values of fluorescence intensity for Ho258 and PI, recorded under the different excitation conditions in G_1 and G_0 fibroblasts submitted to single or double staining. Solving equation (14) by introducing these fluorescence values, the mean FRET efficiency values estimated all over the nuclei were 11.5% and 17.9% for G_0 and G_1 fibroblasts, respectively.

The FRET calculation procedure described above cannot be applied to the case of fibroblasts released from the quiescent state, since the cell population heterogeneity does not allow dye-DNA concentration to be evaluated through a binding study.

Due to the relationships:

$$_{405}FI(A)_{630} = C(A) \cdot \varepsilon(A)_{546} \cdot \phi \cdot I_0, \text{ and}$$
$$_{405}FI(D)_{480} = C(D) \cdot \varepsilon(D)_{405} \cdot \phi \cdot I_0$$

the ratio of the dye concentrations can be derived from the fluorescence intensity values for each double stained cell, provided that the excitation intensity (I_0), the dye absorption coefficient (ε), and quantum efficiency (ϕ) are known. In this case, FRET analysis is expected to be affected by an error due to the underestimation of the donor emission, because of the quenching caused by energy transfer. This was verified on G_0 and G_1 cells. Following this calculation procedure, the percentage of increase in FRET efficiency of G_1 in comparison with G_0 cells was 61% in comparison with 56%, as evaluated according to the concentration ratios derived from the binding studies. Evaluation of FRET efficiency on fibroblasts during the release from quiescent state by using fluorescence intensities showed an increase in the FRET efficiency values already at 60 min after addition of 10% serum, to reach at 20h a value that approaches that of G_1 cells (Figure 1).

FRET imaging

FRET efficiency distribution in nuclei in G_0 and G_1 conditions was evaluated by means of imaging analysis procedure based on equation (14), taking into account that the dye concentration ratio must be calculated pixel-by-pixel because of the heterogeneity of dye distribution within the nucleus. This can be obtained by substituting the term $[C(A)/C(D)]$ of equation (14) with the ratio of the fluorescence images $[(I_{546/630\ corrected}) / (I_{405/480\ corrected})]$ multiplied by a calibration constant (C) which normalizes the fluorescence intensities to the dye concentration:

$$C = \frac{\Sigma_n\, I_{n\ 405/480\ corrected}}{\Sigma_n\, I_{n\ 546/630\ corrected}} \cdot \frac{[PI\text{-}DNA]}{[Ho258\text{-}DNA]} \qquad \textbf{(15)}$$

Table 5. Microspectrofluorimetric analysis. Fluorescence intensities were evaluated on cells after single or double staining with Ho258 and PI.

Cell growing phase	$_{405}Ho_{480\pm10\ nm}$	$_{546}PI_{630\pm10\ nm}$	$_{405}Ho/PI_{480\pm10nm}$	$_{546nm}Ho/PI_{630\pm10\ nm}$	$_{405}PI_{630\pm10nm}$	$_{405}{}^*PI_{630\pm10nm}$
G_0	47,000	22,600	43,600	17,050	3,740	1,193
G_1	48,900	19,750	43,700	18,650	5,155	1,305

**Acceptor direct emission values, obtained from $_{546}Ho/PI_{610}$ values. At least 50 cells measured for each condition. S.E. ≤ 3%.*

where $\Sigma_n I_{n\,\lambda exc/\lambda em\ corrected}$ is the pixel-by-pixel summed emission value of the donor or acceptor image, and [dye-DNA] is the concentration value evaluated by means of the binding kinetics studies.

Typical examples of calculated FRET images of G_0 and G_1 fibroblasts are shown in Figure 4. The presentation in false colors suggests that FRET distribution is more heterogenous in G_1 than in G_0 cells, as confirmed by the asymmetry parameters values (1.1 and 1.7, respectively) calculated on the distribution histograms of FRET efficiency values (Figure 5).

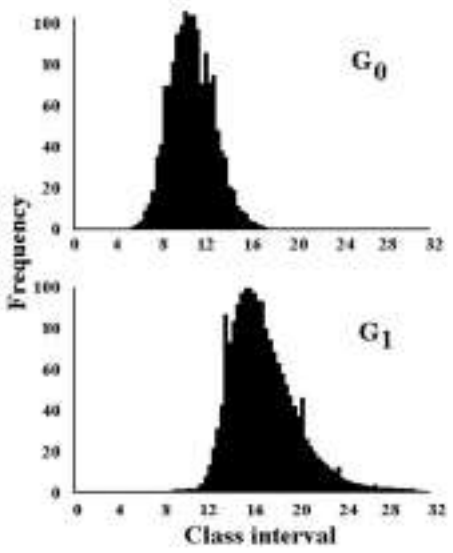

Figure 5. Distribution histograms of the FRET efficiency values from the images of G_0 and G_1 fibroblasts shown in Figure 4.

Discussion

According to Forster's theory, the efficiency of the FRET process is dependent on geometric and spectroscopic variables (Forster, 1948); in solution, all the conditions can be well defined, so that a strictly quantitative evaluation of FRET efficiency as well as the calculation of the absolute Forster's critical distance can be obtained. At the cellular level, on the contrary, limitations exist due to both the experimental apparatus, requiring an accurate calibration of the optical elements and a high detector sensitivity (Ludwing et al., 1992), and to the difficulty to estimate some of the theoretical variables of the complete Forster's expression.

An *in situ* FRET estimation can be obtained through time resolved measurements, or the quenching of the donor, or the sensitised emission of the acceptor. All these methods suffer for some drawbacks. Time resolved fluorescence imaging FRET analysis (Gadella et al., 1993; Murata et al., 2000a) has the advantage of being independent from the concentration measurement, but a sophisticated instrumentation is required for both excitation and measurements.

The quenching of the donor is affected by environmental factors, including the concentration of the fluorochromes used. An overestimation of FRET can occur in fluorescence imaging, due to the heterogeneity of the efficiency values of the different pixels and the need of obtaining averaged values, since a comparative analysis of the quenching kinetics is performed between single and double stained samples (Jovin 1989, Song et al., 1996; Nagy et al., 1998).

Overlap of the donor and acceptor emission spectra or the direct excitation of the acceptor at the donor excitation wavelength could affect in particular FRET estimate through the acceptor sensitised emission. This would require the correction for spillage factors, to be calculated from single stained samples (Matkò et al., 1988). However, thanks to the availability of dye pairs with favourable photophysical properties and to the proper selection of staining conditions, spectral cross-talks may become negligible and the need for correction be minimized. To this aim, in this work the excitation at 405 nm was used, which corresponds to the lowest PI absorption value, while providing a still adequate excitation of Ho258 (Latt and Wohlleb 1975, Bottiroli et al., 1989).

There are several examples of application of FRET-based techniques to study chromatin DNA organization (Sahar and Latt, 1980; Latt et al., 1980; Langlois and Jensen, 1979; Ronchetti et al., 1997; Murata et al., 2003). This is however the first time that this approach has been used to investigate a key process in cell cycle progress, i.e. the transition from the G_0 quiescent phase to the G_1 pre-DNA-synthetic phase. It is of potential interest to detect precociously, within heterogeneous cell populations, the presence of potentially proliferating cells, especially in those biological conditions (such as some early cancers) in which the occurrence of G_0-G_1 transition is an expected event. To this purpose, the cytochemical and cytometric analyses *in situ* must still be considered as an unique approach to identi-

fy minor cell fractions.

FRET efficiency is lower in G_0 than in G_1 fibroblasts: this is likely due to a higher chromatin packaging in quiescent cells which especially hinders the intercalation of PI molecules, thus making the interaction with the donor molecules less favorable, in terms of relative distance and spatial orientation. In fact, a reduction of the dye fluorescence intensities occurs in double stained samples, with respect to the single stained ones, that may be generally due to reciprocal partial hinderance. The reduction in the values of PI is more evident in G_0 than in G_1 cells, suggesting a greater hindering effect of Ho258 on PI intercalation in resting fibroblasts, likely due to their relatively higher chromatin condensation (Leitch, 2000); the reduction in the donor fluorescence intensity can be mainly ascribed to the energy transfer phenomenon.

Interestingly enough, FRET efficiency significantly increased shortly (1h) after serum stimulation of quiescent fibroblasts, thus indicating that chromatin is rearranged in parallel with activation of cycle-related gene; this seems to occur almost synchronously in the whole cell population, consistent with the data on the activation of early-G_1 genes such as c-jun and c-fos (Bravo, 1990).

It is worth noting that FRET signs of occurred G_0-G_1 transition are detected very early compared to another well accepted marker of proliferation potential, i.e. the immunopositivity for the nuclear antigen Ki-67, which in our cell model start to increase 24h after serum stimulation.

The G_1-related changes in FRET efficiency are again due to changed chromatin superstructure, as also suggested by our results after DNase I digestion *in situ* (personal, unpublished observation): the higher availability of G_1-chromatin DNA to the enzyme cleavage may be accounted for by the decondensation of chromatin due to gene activation, consistent with the generally accepted concept (see Holde and Zlatanova, 1996) that the spatial reorganization of chromatin during gene activation may play a significant role in regulating transcriptional activity.

In addition, our results following FRET imaging demonstrate that local chromatin restructuring apparently occurs and gives rise to micro-heterogeneities in the nuclear organization.

FRET-based analyses which already proved to be suitable for studying the overall chromatin organization in differentiated cells (Bottiroli et al., 1989, 1992, 1994; Ronchetti et al., 1997; Murata et al., 2000a; Zuccotti et al., 1994), may now be envisaged as a powerful tool for detecting, in single cells, more subtle changes linked to the activation of early cycle-related genes.

In the present work the ratios of dyes concentrations to be introduced in equation (14) were estimated on G_0 and G_1 cells from the number of binding sites, that were evaluated on parallel samples, because in these cases the amount of DNA per cell is constant. In view of further applications of FRET efficiency calculation, it is to note that, provided that the quenching of the donor is small, the possibility of using only fluorescence values to apply equation (14) gives a reliable information useful to compare samples under different biological conditions. This opens new perspectives for FRET analysis when the concentration parameters required by equation (14) cannot be defined directly. This could occur with cells exhibiting variable DNA amounts, such as populations with heterogenous ploidy or apoptotic cells, in which DNA is progressively cleaved by endonucleases. The simplified FRET calculation may be also applied for flow cytometric analyses, since the measurements of parameters required for FRET calculation are performed on the same single cells.

Acknowledgments

The authors wish to thank Ms. Paola Veneroni for the skilful technical assistance in cell culture.

Funding

This work was supported in part by the Italian MIUR (C.P: Cofin 2002 project).

References

Bottiroli G, Croce AC, Gerzeli G, Barni S. DNA double-staining for a fluorescence energy transfer study of chromatin in liver cells. Cell Biophys 1989;15:249-263.

Bottiroli G, Croce AC, Pellicciari C, Ramponi R. Propidium iodide and the thiol-specific reagent DACM as a dye pair for fluorescence resonance energy transfer analysis: an application to mouse sperm chromatin. Cytometry 1994;15:106-16.

Bottiroli G, Croce AC, Ramponi R. Fluorescence resonance energy transfer imaging as a tool for in situ evaluation of cell morphofunctional characteristics. J Photochem Photobiol B: Biol 1992;12:413-6.

Bravo R. Genes induced during the G_0/G_1 transition in mouse fibroblast. Seminars in Cancer Biol 1990;1:37-46.

Clegg R. Fluorescence resonance energy transfer, In: Wang XF, Herman B, editors. Fluorescence imaging spectroscopy and microscopy. John Wiley, New York, 1996. p. 179-252.

Cosa G, Focsaneanu KS, McLean RN, McNamee JP, Scaiano JC. Photophysical properties of fluorescent DNA-dyes bound to single- and double-stranded DNA in aqueous buffered solution. Photochem Photobiol 200173:585-99.

Dale RE, Eisinger J. Polarized excitation energy transfer. In: Chen RF, Edelhoch H, eds. Biochemical Fluorescence. Concepts, vol. 1. Marcel Dekker Inc.: New York; 1975: p. 115-284.

Endl E, Steinbach P, Knuchel R, Hofstadter F. Analysis of cell cycle-related Ki-67 and p120 expression by flow cytometric BrdUrd-Hoechst/7AAD and immunolabeling technique. Cytometry 1997; 29:233-41.

Forster T. Intramolecular energy migration and fluorescence. Ann Physic 1948;2:55-75.

Gadella TWJ, Jovin TM, Clegg RM. Fluorescence lifetime imaging microscopy (FLIM): spatial resolution of microstructures on the nanosecond time scale. Biophys Chem 1993;48:221-39.

Gordon GW, Berry G, Liang XH, Levine B, Herman B. Quantitative fluorescence energy transfer measurements using fluorescence microscopy. Biophys J 1998;74:2702-13.

Heim M, Tsien RY. Engineering green fluorescent protein for improved brightness, longer wavelengths and fluorescence resonance energy transfer. Curr Biol 1996; 6:178-82.

van Holde K, Zlatanova J. What determines the folding of the chromatin fiber? Proc Natl Acad Sci USA 1996;93:10548-55.

Jovin TM, Arndt-Jovin D. FRET microscopy: Digital imaging of fluorescence resonance energy transfer. Application in cell biology. In: Kohen E, Hirschberg JG, eds. Cell Structure and Function by micro-spectrofluorometry. Academic Press: San Diego; 1989. p. 99-117.

Kam Z, Volberg T, Geiger B. Mapping of adherens junction components using microscopic resonance energy transfer. J Cell Sci 1995;108: 1051-62.

Kim M, Carman CV, Springer TA. Bidirectional transmembrane signaling by cytoplasmic domain separation in integrins. Science 2003; 301:1720-5.

Langlois RG, Jensen RH. Interaction between pairs of DNA-specific fluorescence stains bound to mammalian cells. J Histochem Cytochem 1979;27:72-9.

Lanni C, Bottone MG, Bardoni A, Dyne K, Soldani C, Pellicciari C, et al. Proliferation characteristics and polyploidization of cultured myofibroblasts from a patient with fibroblastic rheumatism. Eur J Histochem 2003;47:257-62.

Latt SA, Wohlleb JC. Optical studies of the interaction of 33258 Hoechst with DNA, chromatin, and metaphase chromosomes. Chromosoma 1975;52:297-316,

Latt SA, Juergens LA, Matthews DJ, Gustashav KM, Sahar E. Energy transfer-enhanced chromosome banding. An overview. Cancer Gen Cytogen 1980;1:187-96.

Le Pecq JB, Paoletti C. A fluorescent complex between ethidium bromide and nucleic acids. J Mol Biol 1967;27: 87-106.

Leitch A.R. Higher level of organization in the interphase nucleus of cycilng and differentiated cells. Microbiol Mol Biol Rev 2000;64: 138-52.

Locatelli D, Delmonte Corrado MU, Politi H, Bottiroli G. Application of fluorescence resonance energy transfer techniques to the study of lectin-binding site distribution on Paramecium primaurelia (protista, Ciliophora) cell surface. Eur J Histochem 1998;42:205-12.

Ludwing M, Hensel NF, Hartzman RJ. Calibration of a resonance energy transfer imaging system. Biophys J 1992;61:845-57.

Mangiarotti R, Bottone MG, Danova M, Pellicciari C. Bivariate flow cytometric analysis of DNA content versus immunopositivity for ribonucleotide reductase M1 subunit in the cell cycle. Cytometry 1998;32:78-85.

Marshall AG. Chemical reactions and equilibrium constants. In: Marshall AG, editors. Biophysical Chemistry. Principles, Techniques, and Applications. John Wiley & Sons: New York, Brisbane, Toronto, Chichester; 1978. p. 51-86.

Matkò J, Szöllõsi J, Trón L, Damjanovich S. Luminescence spectroscopic approaches in studying cell surface dynamics. Q Rev Biophys 1988;21:479-544.

Murata S, Herman P, Lin HJ, Lakowicz JR. Fluorescence lifetime of nuclear DNA: Effect of fluorescence resonance energy transfer. Cytometry 2000;41:178-85.

Murata S, Kusba J, Piszczek G, Gryczynski I, Lakowicz J. Donor fluorescence decay analysis for energy transfer in double-helical DNA with various acceptor concentrations. Biopolymers (Biospectroscopy) 2000b;57:306-15.

Murata S, Herman P, Mochikuzi K., Nakazawa T, Kondo ., Nakamura N, et al. Spatial distribution analysis of AT- and GC-rich regions in nuclei using corrected fluorescence resonance energy transfer. J Histochem Cytochem 2003;51:951-8.

Nagy P, Vámosi G, Bodnár A, Lockett SJ, Szöllõsi J. Intensity-based energy transfer measurements in digital imaging microscopy. Eur Biophys J 1998;ì27:377-89.

Pellicciari C, Mangiarotti R, Bottone MG, Danova M, Wang E. Identification of resting cells by dual parameter flow cytometry of statin expression and DNA content. Cytometry 1995;21:329-37.

Price NC, Dwek RA Binding of ligands to macromolecules. In: Price NC, Dwek RA, eds. Principles and Problems in Physical Chemistry for Biochemists. Clarendon Press: Oxford; 1979. p. 33-43.

Ronchetti E, Bottiroli G, Curti S, Formenti D, Pellicciari C, Manfredi Romanini MG. Occurrence of DNA sequence differences in C-heterochromatin of Eulemurcoronatus and Eyulemur macaco as revealed by fluorescence resonance energy transfer. Eur J Histochem 1997;41:79-90.

Sahar E, Latt SA. Energy transfer and binding competition between dyes used to enhance staining differentiation in metaphase chromosomes. Chromosoma 1980;79:1-28.

Santisteban MS, Brugal G. Fluorescence image analysis of the MCF-7 cycle related changes in chromatin texture. Differences between AT- and GC-rich chromatin.Anal Cell Pathol 1995;9:13-28.

Schiller PW. The measurements of intramolecular distances by energy transfer. In: Chen RF, Edelhoch H, eds. Biochemical Fluorescence: Concepts, Vol 1,. Marcel Dekker: New York; 1975. p. 285-303.

Song L, Varma CA, Verhoeven JW, Tanke HJ. Influence of the triplet excited state on the photobleaching kinetics of fluorescence microscopy. Biophys J 1996;70:2959-68.

Stryer L. Fluorescence energy transfer as a spectroscopic ruler. Ann Rev Biochem 1978;47:819-46.

Szöllõsi J, Damjanovic S, Mátyus L. Application of fluorescence energy transfer in the clinical laboratory: Routine and research. Cytometry 1998;34:159-79.

Szöllõsi J, Mátyus L, Balazs M, Ember I, Fulwyler M, Damjanovich S. Flow cytometric measurements of fluorescence energy transfer using single laser excitation. Cytometry 1987;8:120-8.

Szöllõsi J, Tron L, Damjanovic S, Helliwell SH, Arndt-Jovin D, Jovin T. Fluorescence energy transfer measurements on cell surface: a critical comparison of steady-state fluorimetric and flow cytometric methods. Cytometry 1984;5:210-6.

Uster PS, Pagano RE. Resonance energy transfer microscopy: observation of membrane-bound fluorescent probes in model membranes and in living cells. J Cell Biol 1986;103:1221-34.

Zuccotti M, Katayose H, Matsuda J, Redi CA, Bottiroli G, Yanagimachi R. Fluorescence energy transfer shows that various physical and chemical treatments of human sperm induce unpacking of chromatin. Andrologia 1994;26:225-30.

Wang E. A 57,000-mol-wt protein uniquely present in nonproliferating cells and senescent human fibroblasts. J Cell Biol 1985a;100:545-51.

Wang E. Rapid disappearance of statin, a nonproliferating and senescent cell-specific protein, upon reentering the process of cell cycling. J Cell Biol 1985b;101:1695-701.

Wang E, Krueger JG. Application of a unique monoclonal antibody as a marker for nonproliferating subpopulations of cells of some tissue. J Histochem Cytochem 1985;33:587-94.

Wang E, Lin SL. Disappearance of statin, a protein marker for non-proliferating and senescent cells, following serum-stimulated cell cycle entry. Exp Cell Res 1986;167:135-43.